Hindawi
Advances in Civil Engineering
Volume 2021, Article ID 9958436, 13 pages
https://doi.org/10.1155/2021/9958436

*Research Article*

# Experimental Analysis of Bending Stiffness Characteristics of Grouted Double Mortise-Tenon Joint for Prefabricated Metro Station Structure

**Xiuren Yang**[1,2], **Fang Lin**[1,2] **and Meiqun Huang**[1,2]

[1]*Beijing Urban Construction Design and Development Group Co., Ltd., Beijing 100037, China*
[2]*National Engineering Laboratory for Green & Safe Construction Technology in Urban Rail Transit, Beijing 100037, China*

Correspondence should be addressed to Xiuren Yang; yangxr@bjucd.com and Fang Lin; felyo@foxmail.com

Received 5 March 2021; Revised 29 March 2021; Accepted 14 June 2021; Published 23 June 2021

Academic Editor: Rihong Cao



The grouted mortise-tenon joint, invented as the connection between the large prefabricated components, is the key to the prefabricated underground structures, and the double-tenon joint is most widely used in the prefabricated metro station structure. This paper conducts characteristic analysis of bending stiffness with a 1 : 1 prototype test in key working direction of different joint types for grouted double mortise-tenon joint. The results show that the double-tenon joint is characteristic of variable stiffness under different loads. Change laws of double-tenon joint bending stiffness without and with auxiliary pretightening device in tension side and compression side are also discussed. The correlations for calculating double-tenon joint bending stiffness with various axial loads and bending moments are derived at last, which offers the theory foreshadowing of similar joints.

## 1. Introduction

With the rapid development of rail transit construction in China, social-environmental awareness increases continuously. Moreover, long and tight construction period, large resource consumption, decrease of young laborers of civil engineering causing shortage of skilled labor, and not guaranteed structure quality bring great challenges to traditional construction technology of metro station. The above situations are particularly prominent in the northeast of China like Changchun city, located in the northeast region, which is so cold that 4~5 months' winter break is needed for metro construction, which causes huge deadline pressure and is hard to guarantee construction quality under low temperature [1–4].

To address these problems, a new prefabricated technology has been researched, developed, and implemented by Yang et al. team for constructing metro stations [5–7]. Shuangfeng Station on Changchun Metro Line 2 was selected in 2012 as a test station to conduct systemic research and develop the prefabrication technology for designing underground metro station structures. The prefabricated structure has significant advantages of high efficiency, high quality, and green and environmental protection. For now, 6 prefabricated metro stations have been completed.

The six cut-and-cover stations are all supported by an anchor-pile system. All those horseshoe-shaped two-storey stations are 20.5 m wide and 17.45 m high. The full prefabricated station structure is assembled by seven 2 m width prefabricated components (see Figure 1) without any concrete wet spraying. The grouted double-tenon joint is the most widely used joint connection method in the prefabricated station structure of Changchun Metro Line 2 (see Figure 1). The joint performance of a prefabricated metro station has an important impact on the mechanical properties of the whole structure [5–7]. The bending stiffness (rotational stiffness) of the joint is one of the main factors that directly affect the distribution of internal force (especially bending moment) of the structural system. Its stiffness presents a complex mechanical relationship, which changes with the load atmosphere, joint type and size, and other factors.

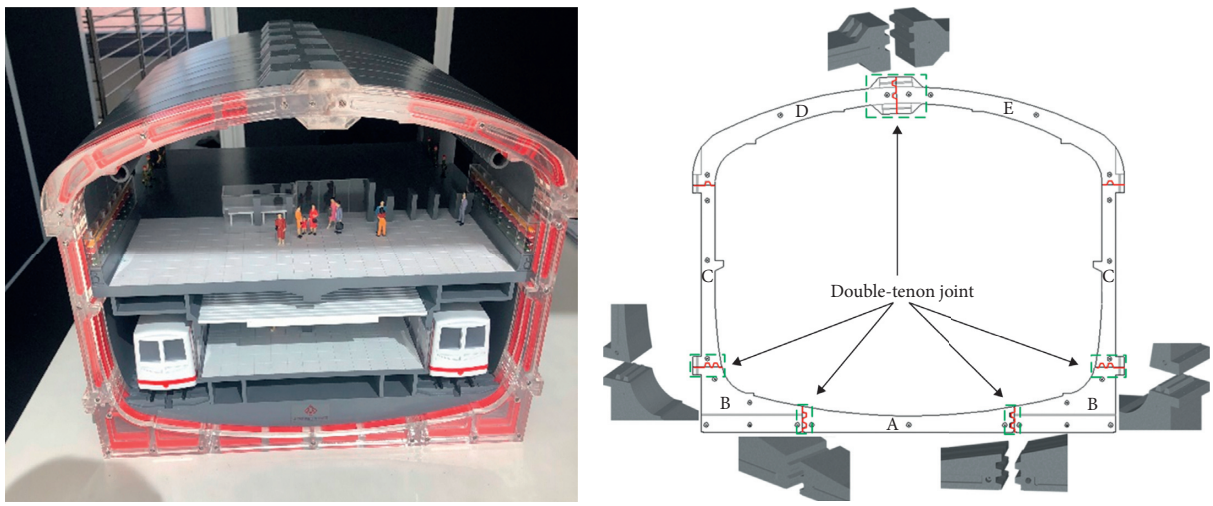


(a) (b)

Figure 1: Prefabricated metro station display and arrangement of grouted double-tenon joint.

In the past, scholars have carried out a more in-depth study on the mechanical behavior of shield tunnel segment joints [8–11], but due to the great differences in the structural type, connection method, and loading process of prefabricated station, the research results of shield tunnel cannot be directly applied [12–15]. Therefore, the research team independently developed a set of comprehensive test systems which can be used for prototype or large-scale component joint test [16]. Taking the joint used in Changchun prefabricated station as the research object, the mechanical properties of grouted mortise-tenon joint were studied through prototype test. Based on the test data, this paper analyzes the bending stiffness characteristics of grouted double-tenon joint and puts forward the relevant empirical calculation formula of bending stiffness of the joint. It is the first time to study the characteristics of the newly developed joint for the new prefabricated underground structure, and it is very helpful for engineering application.

## 2. Test Scheme

In this study, the bending properties of three kinds of grouted double-tenon joints under various axial loads were tested, including (1) the joint without auxiliary pretightening device; (2) the joint with auxiliary pretightening device in tension side; (3) the joint with auxiliary pretightening device in compression side. The test conditions and loading mode are shown in Table 1. The auxiliary pretightening device is composed of the pretightening steel bar and a boss, as shown in the blue dotted box in Table 1. The specimen is 1 : 1 prototype size along the key loading direction (cross-section direction shown in Figure 1), and the actual width of 2000 mm is taken as 500 mm along the nonkey loading direction.

In the test, the edge measurement method is used to indirectly measure the joint rotation angle (as shown in Figure 2). The angle $\theta$ is calculated by the values of $A$ and $B$ measured by the draw-wire displacement sensors and the carrier rod displacement sensors arranged on the top surface and two sides of the joint specimen. The calculation formula is as follows:

$$\begin{cases} A \times X_2 = B \times X_1, \\ \sin\dfrac{\theta}{2} = \dfrac{B}{2X_2}, \\ X_1 + X_2 = \dfrac{1.02}{1.42}, \\ \left(\dfrac{\text{without}}{\text{with auxiliary pretightening device}}\right). \end{cases} \tag{1}$$

## 3. Analysis of Test Results

*3.1. Joint Resistance Bending Moment.* The main structural components of prefabricated metro station are in an eccentric compression state. For the joint interface, compression effects of axial force, the connection force of joint (such as the force of steel bar, the bond force of interface, etc.), and the embedment of long tenon are a pair of equilibria corresponding to the bending action of the joint. The bending moment formed by the axial force, the joint connection force, and the embedment effect of the long tenon in bending deformation are used to resist the bending moment of the joint. It is an important factor to keep the joint stable, which we call the "resistance" of the joint.

The expression of "resistance" is $M = M_R + M_{R2} + M_{R3} + M_{R4}$, including the following:

(a) The resistance moment (resistance caused by the active force) formed by the axial force of the components changes with the axial force, and the

Table 1: Test cases and layout.

| | | |
|---|---|---|
| Cases | Axial load: 0 kN, 500 kN, 1000 kN, and 1250 kN | Without auxiliary pretightening device<br> 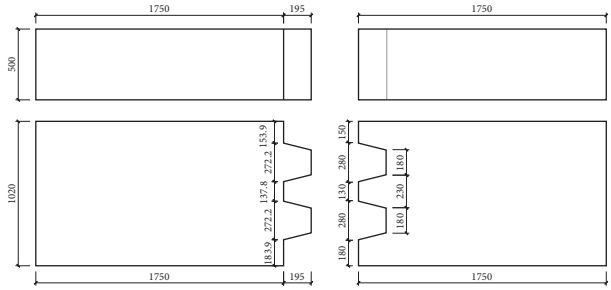 <br>With auxiliary pretightening device<br> 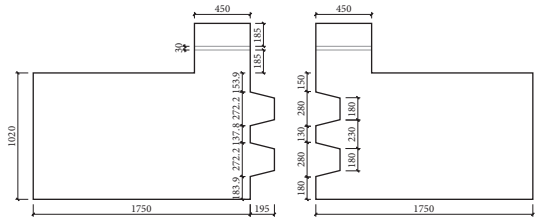 |
| Test content | | The amount of opening and compression of the joint (so as to obtain the joint rotation angle); the whole process record of crack development details of the joint |
| Loading layout | | 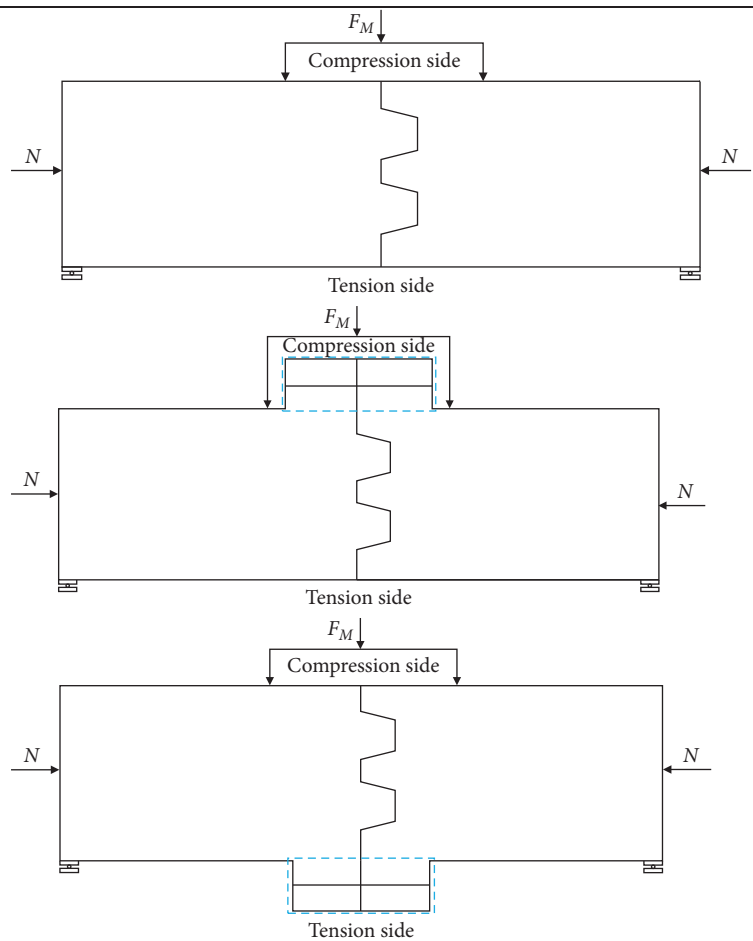 |

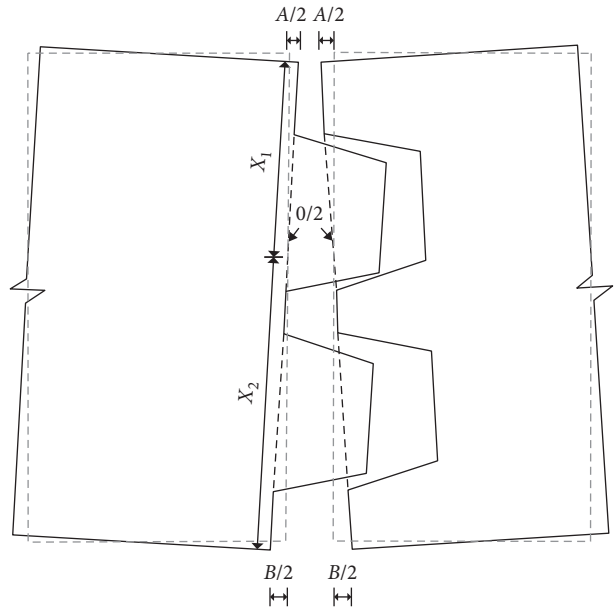


Figure 2: Measurement method for rotation-displacement of grouted double-tenon joint.

resistance moment $M_R$ can be calculated according to Figure 3 with the following formula:

$$M_R = N \cdot l_R, \tag{2}$$

where $M_R$ is the resistance moment formed by axial force; $N$ denotes the axial force; $l_R$ represents the resistance arm, taking $h/2$ as the length of the contact surface of the joint (i.e., grouting length).

(b) The resistance force $M_2$ caused by the joint connecting steel bar includes the pretightening moment of the steel bar and the moment formed by the tensile force of the steel bar at the joint opening side caused by the opening (or compression) of the joint under loading (the pretightening force of the steel bar is relaxed for the compressed side). This part of resistance can be calculated according to the following formula in Figure 4:

When $T_0 > N$, the pretightening effect of the steel bar is not completely offset by the compressive stress generated by the axial force; here, $M_2 = T \cdot h_T$. $T_0$ is the initial pretightening force. $T$ is the actual pretightening force. $T$ is a positive value when the steel bar is located in tension side, and it is a negative value when the steel bar is located in compression side.

When $T_0 \leq N$, the steel bar is relaxed ($T = 0$), and the pretightening effect of the steel bar can be ignored.

(c) Due to the low tensile strength of concrete, the resistance of $M_{3-1}$ caused by bond strength of the joints can be negligible.

(d) The mortise and tenon of the joint embedded together can also provide a certain resistance under the action of bending moment. In calculation, the moment $M_4$ (when there is bending effect of tenon) and (or) the moment $M_{3-2}$ formed by the bond action between mortise and tenon can be included according to the actual stress trend. Because the two tenons of the double-tenon joint are located at the core of the tension and compression area under the bending action, the tenon bears the tension and compression effect, and the bending effect is weak, so the embedment effect between mortise and tenon cannot be considered. Considering the low bond strength between mortise and tenon, the tension and compression effect can also be ignored.

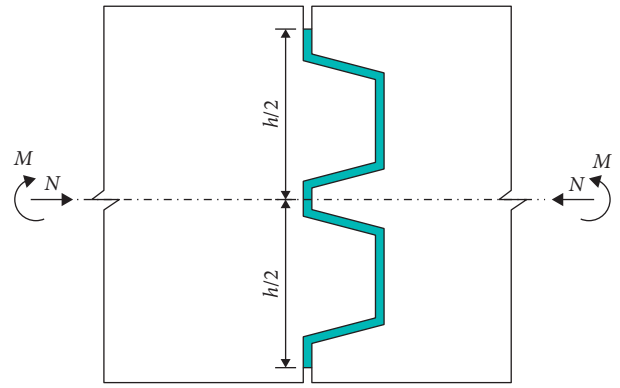


Figure 3: Calculation model of resistance bending moments $M_R$.

The joint resistance, especially the resistance moment, is an important index to analyze the mechanical behavior of the joints.

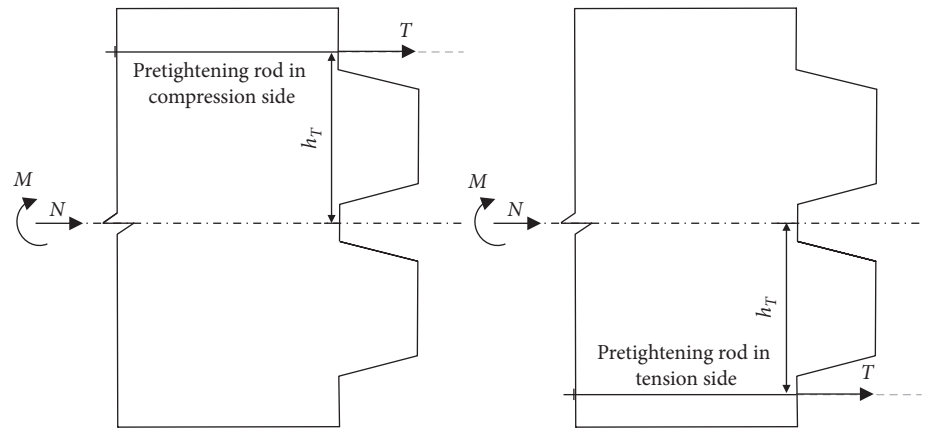


Figure 4: Calculation model of resistance $M_R$ from pretightening rod.

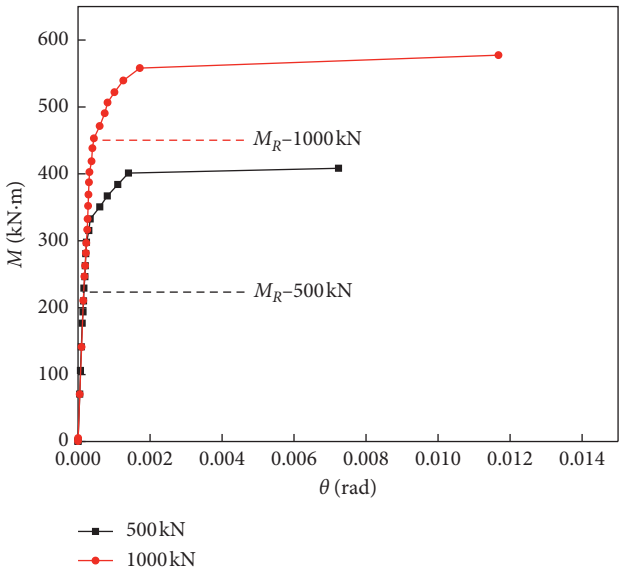


Figure 5: Comparison of $M$–$\theta$ relationship curve for double-tenon joint without auxiliary pretightening device under different axial loads.

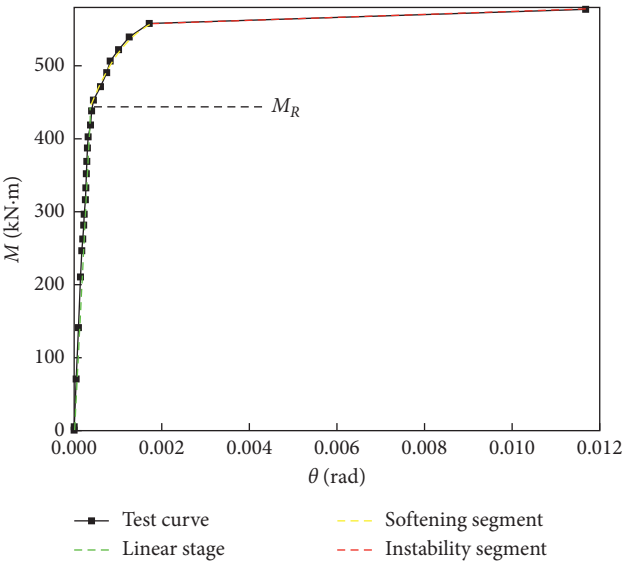


Figure 6: $M$–$\theta$ relationship curve of double-tenon joint without auxiliary pretightening device under axial load 1000 kN.

### 3.2. Bending Moment: Rotation Relationship of Double-Tenon Joint under Different Working Conditions

*3.2.1. Joint without the Auxiliary Pretightening Device.* According to the joint rotation angle $\theta$ obtained from the test under different axial loads and bending moments, the $M$–$\theta$ relationship curve of the grouted double-tenon joint without auxiliary pretightening device is shown in Figure 5.

It can be found that $M$–$\theta$ curve is composed of linear segment and one (or more) nonlinear segment. The axial force has a great influence on the $M$–$\theta$ curve, and its bending capacity is proportional to the axial force.

Through in-depth analysis of $M$–$\theta$ curve (see Figure 6), it is found that the straight segment (linear segment) corresponds to the stage in which the joint remains intact without any damage (or very slight damage), and the bending moment loading value at this stage is basically equivalent to the joint resistance moment. When the bending moment loading value exceeds the resistance moment, the joint cracks appear and develop with the increase of bending moment. The integrity of the joint becomes worse, and the joint softens. The $M$–$\theta$ curve enters the nonlinear stage at the same time. At the end of the softening stage, the joint cracks are completely penetrated and rapidly developed, and the joints are subject to transient failure and completely lose the bearing capacity.

After clarifying the physical meaning of the above joint behavior, we can divide the $M$–$\theta$ curve of the joint loading process into three stages:

(a) Linear stage: in this stage, the peak load moment does not exceed the resistance moment of the joint. The joint is not damaged at this stage, and the bending moment is basically linear with the rotation angle. Particularly in the initial stage of loading, there is almost no rotation for the joint surface, and the rotation angle comes from the rotation of the beam.

(b) Nonlinear stage (joint softening stage): the main reason of joint softening at this stage is that the

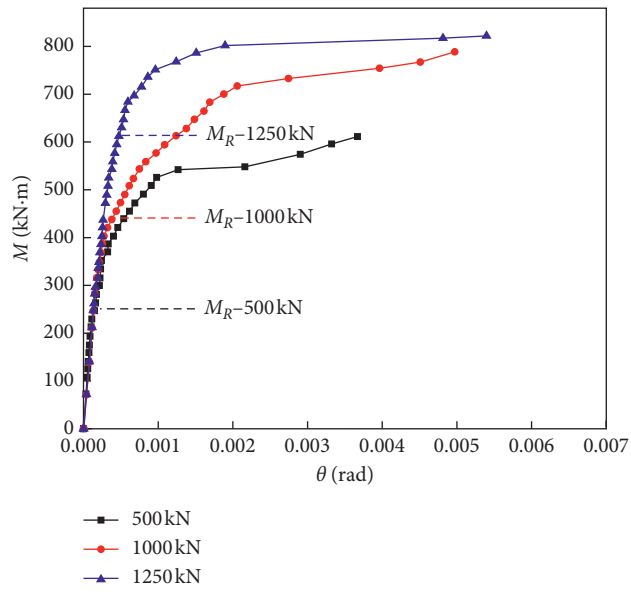


Figure 7: Comparison of $M$–$\theta$ relationship curve for double-tenon joint with auxiliary pretightening device in tension side under different axial loads.

integrity of joint becomes worse after cracks appear in the joint, and the other reason is that the concrete has entered a significant plastic stage.

(c) Joint instability stage: at the end of the softening stage, the cracks of the joint are completely penetrated, transient failure and instability occur in the joint, and the bearing capacity is completely lost. The joint rotation angle develops rapidly. At this time, the $M$–$\theta$ curve is a straight line approximately horizontal. According to the rotational deformation of the joint, with the increase of axial force, the deformation of the joint at the end of the softening stage has a small increase trend, but in the linear stage, the deformation is basically the same regardless of the axial force.

*3.2.2. Joint with the Auxiliary Pretightening Device in Tension Side.* Figure 7 shows the $M$–$\theta$ curve of double-tenon joint of auxiliary pretightening device (two steel bars with diameter of 18 mm) in tension side under different axial loads. It can be seen from the curve that the axial force also has a great influence on the bearing capacity of the joint. The $M$–$\theta$ curve also shows a three-stage distribution similar to that of the joint without auxiliary pretightening device, that is, linear stage, nonlinear stage (joint softening section), and instability stage, but it is also different.

Figure 8 shows the comparison of $M$–$\theta$ curves of joints with and without auxiliary pretightening devices in tension side. The difference can be clearly seen from the figure: the overall bearing capacity of the joint with auxiliary pretightening device is improved (the linear stage is lengthened, and the nonlinear stage is extended). The lengthening of the linear stage is mainly due to the increase of the resistance moment caused by preload of pretightening steel bar. The extension of nonlinear stage is mainly due to the following reasons: (a) The preload of pretightening steel bar provides the unbalanced additional preload on the contact surface of the joint in addition to the axial force (the distribution of the preload is uneven, mainly concentrated near the steel bar). These preloads form a change process from large to small (harmless release section) with the increase of joint bending load, which can delay the occurrence of joint damage. (b) The axial force increases with the opening of the joint, which provides additional resistance moment, delays (reduces) the deterioration process of the joint, and improves the ductility of the joint. It can be seen that the joint rotation is effectively restrained in the nonlinear stage due to the additional tension of the steel bar.

*3.2.3. Joint with the Auxiliary Pretightening Device in Compression Side.* Figure 9 shows the $M$–$\theta$ curve of double-tenon joint of auxiliary pretightening device in compression side under different axial loads. It can be seen from the curve that the axial force still has a great influence on the bearing capacity of the joint. The greater the axial force is, the higher the bearing capacity of the joint is.

There are significant differences in the form of $M$–$\theta$ relationship curve among the joint without auxiliary pretightening device and the joint with auxiliary pretightening device in tension side, which are mainly reflected in the following aspects: (a) the curve shape evolves from the three-stage distribution to the two-stage distribution, which is composed of linear segment and instability failure segment, and the nonlinear segment is significantly shortened or even disappeared; (b) the slope of the linear segment is significantly reduced and changes from the steep shape to the relatively gentle slope state; (c) in the early stage of instability stage, the joint rotation angle becomes smaller and the joint is more likely to be damaged.

Figure 10 shows the comparison of $M$–$\theta$ curves between the auxiliary pretightening device in compression side and in

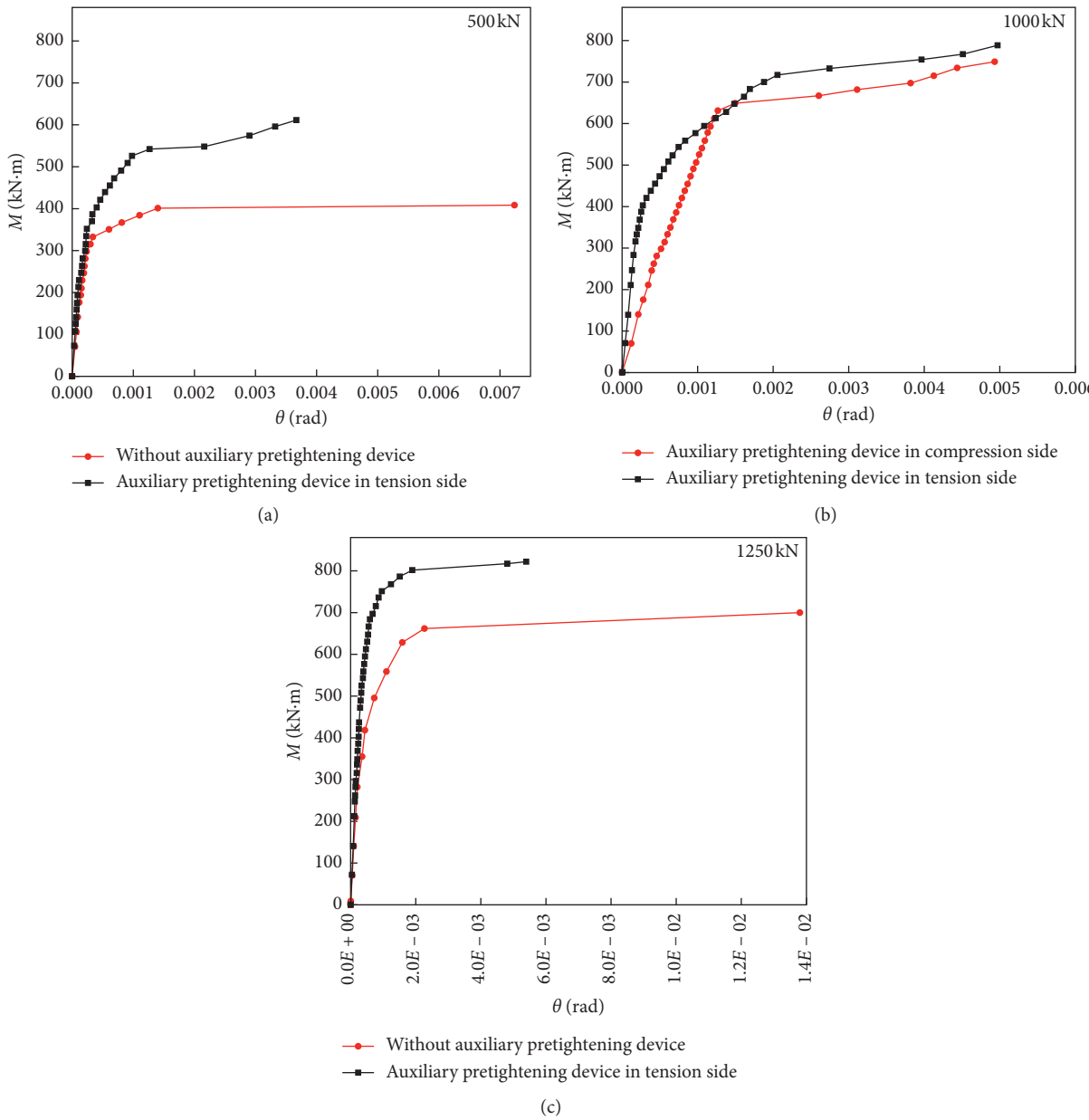


Figure 8: Comparison of $M$–$\theta$ relationship curve for double-tenon joint with and without auxiliary pretightening device under different axial loads.

tension side. It is not difficult to find that the bearing capacity of the auxiliary pretightening device in compression side is lower than that of the auxiliary pretightening device in tension side, and the slope of the linear segment is significantly reduced, which means that the stiffness of the joint is greatly reduced. The nonlinear segment of the joint is longer when the pretightening steel bar is in tension side, which means that the joint has good ductility. However, there is no ductile transition segment in the joint when the pretightening steel bar is in compression side. When the loading reaches the limit, it directly connects with the failure stage. It is found that when the pretightening steel bar is in compression side, the tensile force can form a negative resistance moment (consistent with the bending direction), which will reduce the ability of the joint to bear bending moment. The pretightening steel bar increases the stress of the concrete in compression side, which results in the joint damage ahead of time and reaches the limit faster after loading, the allowable rotation deformation range of the joint decreases, and the overall deformation decreases. Under the same bending moment, the joint rotation is greater than that of the joint with auxiliary pretightening device in tension side.

*3.3. Bending Stiffness Characteristics of Double-Tenon Joint.* The bending stiffness $k_\theta$ ($k_\theta = \mathrm{d}M/\mathrm{d}\theta$, i.e., the loading value of bending moment forming unit rotation angle) reflects the ability of joint to resist bending moment.

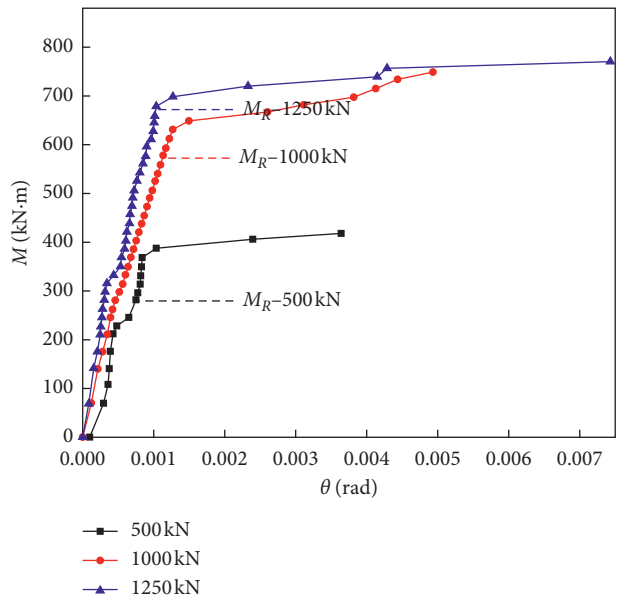


Figure 9: Comparison of $M$–$\theta$ relationship curve for double-tenon joint with auxiliary pretightening device in compression side under different axial loads.

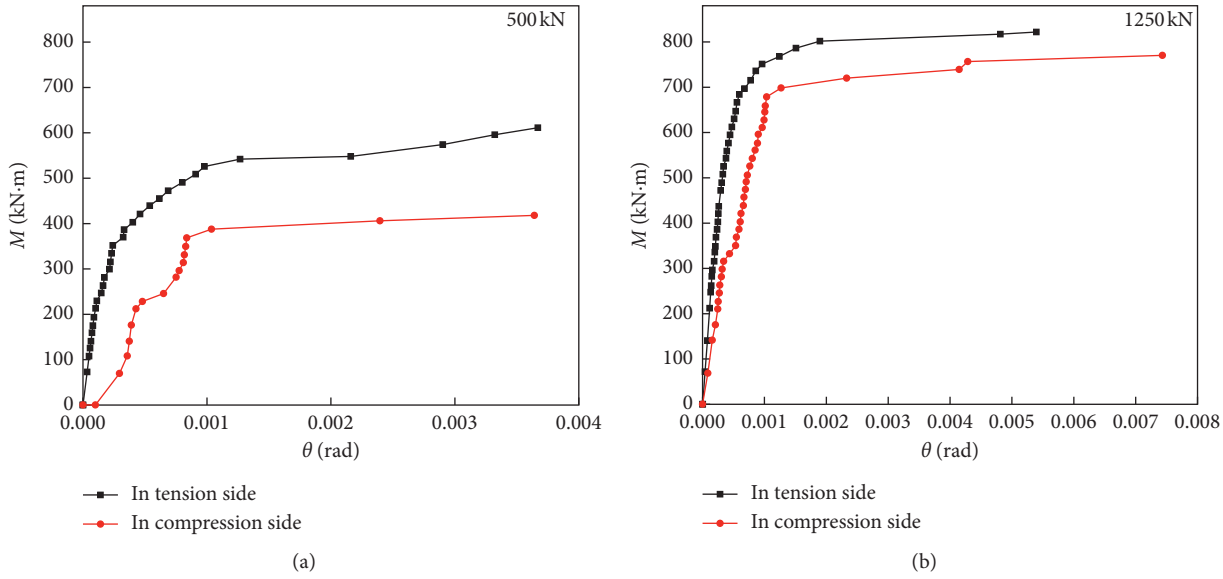


Figure 10: Comparison of $M$–$\theta$ relationship curve for double-tenon joint with auxiliary pretightening device in compression side and without auxiliary pretightening device under different axial loads.

In the past, a fixed value of joint bending stiffness is usually used for structural analysis according to experience in the structural design of shield tunnel. According to the $M$–$\theta$ curve obtained from the joint test under different conditions, it can be seen that the stiffness of the joint does not keep a constant value under different stress conditions, and the bending stiffness characteristics of the joint with the change of the stress environment will have an important impact on the mechanical behavior of the prefabricated structure, so it is very important to master the bending stiffness characteristics of the joint.

In this paper, the $M$–$\theta$ curve obtained from the previous joint test is used to fit the empirical formulas of $M = f(\theta)$, and then according to $k_\theta = \mathrm{d}M/\mathrm{d}\theta$ relationship, the empirical formulas of bending stiffness of joints are obtained, respectively, and the stiffness characteristics of joints are analyzed. On the basis of identifying the key stress points and characteristic points of failure stage, the practical

application range of bending stiffness of different types of joints is proposed.

*3.3.1. Joint without the Auxiliary Pretightening Device.* Using the $M-\theta$ curve of the joint without auxiliary pretightening device, the curve type conforms to the logarithmic function type. Next, according to $k_\theta = \mathrm{d}M/\mathrm{d}\theta$ relationship, the joint bending stiffness curve in the whole loading process is shown in Figure 11, and the fitting stiffness expression is shown in formula (3). The position of key points on the curve, including joint resistance moment (transition point of linear segment and nonlinear segment) and end of nonlinear segment (transition point of joint softening segment and instability segment), is identified in the diagram. Under the condition of small axial load of 500 kN, the transition point of linear segment and nonlinear segment is about 325 kN·m. In addition, in the initial stage of loading ($M \le 140$ kN·m), the rotation is very small, which is basically equal to the rotation angle of continuous beam. In order to avoid the infinite value of $\mathrm{d}M/\mathrm{d}\theta$, the stiffness of continuous beam is used instead. At the end of bearing, because of joint instability, it is not considered as the use stage, and the stiffness calculation formula of this part is not considered. After analysis, the stiffness curve has the following key characteristics:

(a) In the whole loading range, with the change of the load atmosphere, the stiffness of the joint is also in a state of constant change, and the variable stiffness characteristics of the joint are obvious. The specific change trend is as follows: under a certain axial force, the stiffness of the joint decreases with the increase of bending moment. Under the same bending moment, the stiffness of the joint increases with the increase of axial force.

(b) The joint stiffness of load-bearing zone and design utilization zone under different axial loads is present in Table 2.

$$k_\theta = \begin{cases} 91.15 \cdot e^{(1024.2 - M/91.15)} \, (500\,\mathrm{kN}), \\ 145.67 \cdot e^{(1498.1 - M/145.67)} \, (1000\,\mathrm{kN}), \\ 170.26 \cdot e^{(1717 - M/170.26)} \, (1250\,\mathrm{kN}). \end{cases} \quad (3)$$

*3.3.2. Joint with the Auxiliary Pretightening Device.* From the $M-\theta$ curve of Section 3.2.3, it can be seen that the negative resistance moment caused by the auxiliary pretightening device in compression side increases the joint rotation and reduces the joint stiffness compared with the joint without auxiliary pretightening device. In this paper, the stiffness characteristics of the joint with auxiliary pretightening device in tension side are discussed in detail.

The $M-\theta$ curve of the joint with auxiliary pretightening device in tension side also conforms to the logarithmic function type. According to $k_\theta = \mathrm{d}M/\mathrm{d}\theta$ relationship, the joint bending stiffness curve in the whole loading process is shown in Figure 12, and the fitting stiffness expression is shown in formula

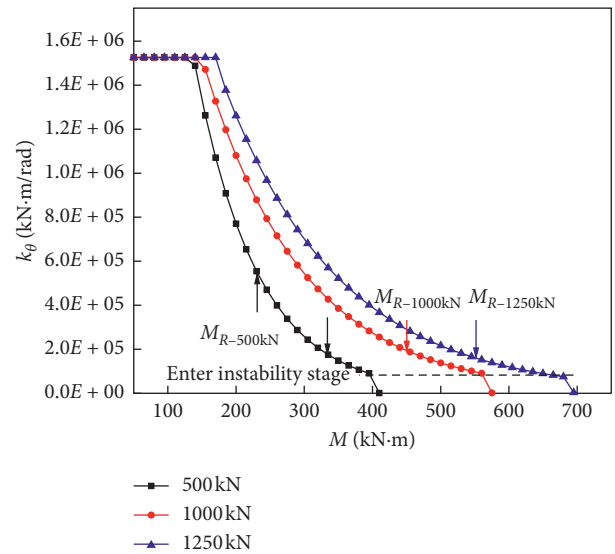


Figure 11: Bending stiffness curve of double-tenon joints without auxiliary pretightening device under different axial loads.

(4). The position of key points on the curve, including joint resistance moment (transition point of linear segment and nonlinear segment) and end of nonlinear segment (transition point of joint softening segment and instability segment), is identified in the diagram. Under the condition of small axial force of 500 kN, the transition point of linear section and nonlinear section is about 380 kN·m. In addition, in the initial stage of loading, the rotation is very small, which is basically equal to the rotation angle of the continuous beam. In order to avoid the infinite $\mathrm{d}M/\mathrm{d}\theta$, the stiffness of the continuous beam is used instead. At the end of the bearing period, because of the instability of the joint, this part of the stiffness calculation formula is not considered. After analysis, the stiffness curve has the following key characteristics:

(a) The characteristics of variable stiffness of the joint are basically consistent with those of the joint without auxiliary pretightening device when the auxiliary pretightening device is located in tension side. However, due to the reinforcement effect of the pretightening steel bar, the joint stiffness is in a constant change state with the change of the load atmosphere, and the variable stiffness characteristics of the joint are obvious. The specific change trend is as follows: under a certain axial force, the stiffness of the joint decreases with the increase of bending moment. Under the same bending moment, the stiffness of the joint increases with the increase of axial force.

(b) The joint stiffness of load-bearing zone and design utilization zone under different axial loads is present in Table 3.

$$k_\theta = \begin{cases} 136.83 \cdot e^{(1468.51 - M/136.83)} \, (500\,\mathrm{kN}), \\ 163.85 \cdot e^{(1722.23 - M/163.85)} \, (1000\,\mathrm{kN}), \\ 241.33 \cdot e^{(2429.8 - M/241.33)} \, (1250\,\mathrm{kN}). \end{cases} \quad (4)$$

Table 2: Design ranges and stiffness values of double-tenon joints without auxiliary pretightening device under different axial loads.

| Axial load (kN) | Design bearing range (kN·m) | Design using bending stiffness (kN·m/rad) |
|---|---|---|
| 500 | 0~325 | $1.96E+05$~$1.53E+06$ |
| 1000 | 0~450 | $1.94E+05$~$1.53E+06$ |
| 1250 | 0~562.5 | $1.52E+05$~$1.53E+06$ |

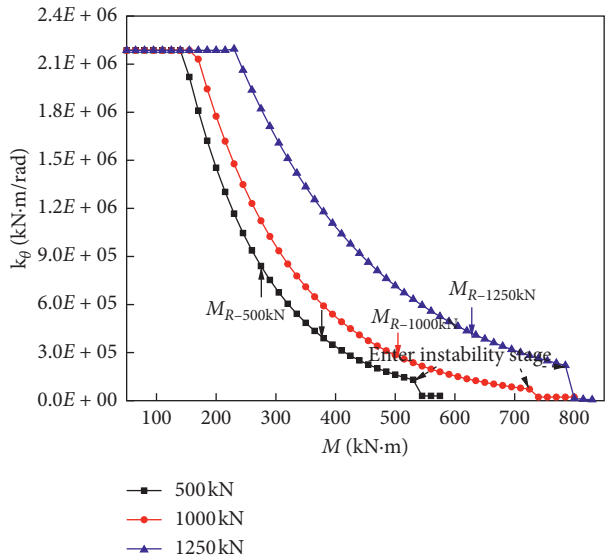


Figure 12: Bending stiffness curve of double-tenon joints with auxiliary pretightening device in tension side under different axial loads.

*3.3.3. Variation Law and Influence Factors of Bending Stiffness*

*(1) Different Axial Loads and Bending Moment Combinations.* According to the empirical formula of bending stiffness fitted by the test, a three-dimensional diagram of the bending stiffness of the double-tenon joint with auxiliary pretightening device in tension side under the combined axial and bending force is drawn, as shown in Figure 13. It can be seen that the bending stiffness of double-tenon joint is affected by both axial force and bending moment and decreases with the increase of the ratio of bending moment to axial force, that is, eccentricity. Under the same axial force, the bending stiffness of double-tenon joint decreases. When the bending moment is small, the bending stiffness is very large and decreases with the increase of bending moment.

It can be seen that the joint reflects the characteristics of variable stiffness, and the bending stiffness increases with the increase of the axial force of the structure and decreases with the increase of the bending moment. In the beginning, the joint stiffness is large, with the bending moment loading exceeding the resistance moment, the joint crack appears, the joint stiffness decreases, and in the later stage of bearing, the permanent crack forms and enters the instability stage and the bending stiffness decreases rapidly.

*(2) Different Types of Double-Tenon Joint.* Figure 14 shows the bending stiffness curves of three types of double-tenon joints under 1000 kN axial force. It can be seen that the bending stiffness of the joint with auxiliary pretightening device in tension side is larger than that of the joint with auxiliary pretightening device in compression side and without auxiliary pretightening device. The bending stiffness of the joint with auxiliary pretightening device in compression side is smaller than that of the joint without auxiliary pretightening device in the initial stage due to the influence of negative resistance moment, and the bending stiffness of the joint with auxiliary pretightening device is gradually greater than that of the joint without auxiliary pretightening device in the middle and late bearing stage.

The joint without auxiliary pretightening device enters the instability stage at the earliest stage (560 kN·m), followed by the joint with auxiliary pretightening device in compression side (680 kN·m), and the joint with auxiliary pretightening device in tension side enters the instability stage at the latest (717 kN·m). At this moment, the bending stiffness is reduced to the order of 4 of 10 and then rapidly decays.

From the view of resistance moment, when the load of the joint without auxiliary pretightening device exceeds the resistance moment of 450 kN·m, the bending stiffness of the joint without auxiliary pretightening device is $1.94E+05$ kN·m/rad, the bending stiffness of the joint with auxiliary pretightening device in compression side is $3.01E+05$ kN·m/rad, and the bending stiffness of the joint with auxiliary pretightening device in tension side is $3.86E+05$ kN·m/rad. It can be seen that the joint with auxiliary pretightening device can delay the stiffness attenuation when the bending moment exceeds the resistance moment; that is to say, the setting of the auxiliary pretightening device is helpful to improve the bending performance of the joint, and it is more advantageous to set the auxiliary pretightening device in tension side regardless of the early and late stages.

Table 3: Design ranges and stiffness values of double-tenon joints with auxiliary pretightening device in tension side under different axial loads.

| Axial load (kN) | Design bearing range (kN·m) | Design using bending stiffness (kN·m/rad) |
|---|---|---|
| 500 | 0~380 | $3.90E+05$~$2.19E+06$ |
| 1000 | 0~490 | $3.02E+05$~$2.19E+06$ |
| 1250 | 0~637.5 | $4.06E+05$~$2.19E+06$ |

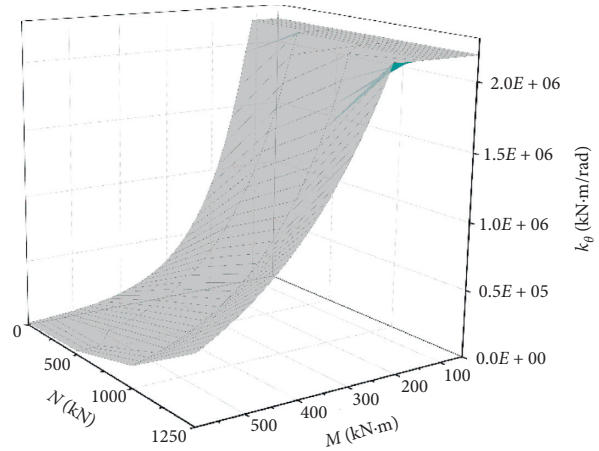


Figure 13: Change law of joint bending stiffness under different axial load and bending moment.

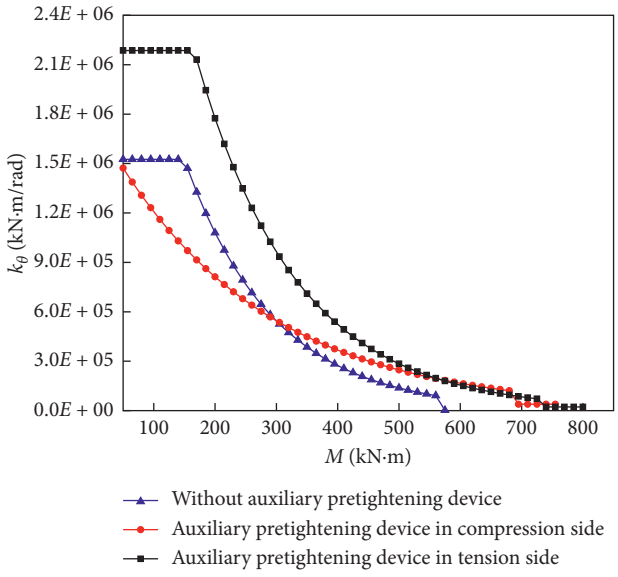


Figure 14: Comparison of joint bending stiffness among different double-tenon joints (1000 kN).

## 4. Empirical Formula of Bending Stiffness of Double-Tenon Joint

Through the analysis of $M$–$\theta$ curves of different types of double-tenon joints under different axial force conditions, the logarithmic function $M = A\ln(\theta) + B$ is used to fit the curves, and $k_\theta = A \cdot e^{(B-M/A)}$ is obtained. Furthermore, the coefficient $A$ and $B$ are fitted and analyzed; that is, the functional relationship between axial force and parameters $A$ and $B$ is analyzed (as shown in Figure 15, the fitting of A and B of the joint without auxiliary pretightening device) is obtained, and the empirical formula of grouted double-tenon joint is shown in Table 4.

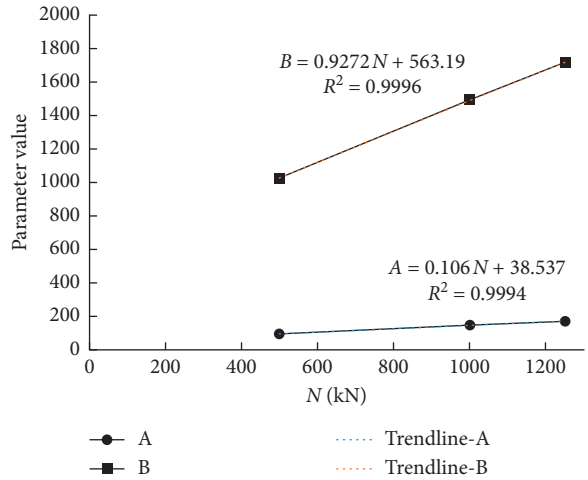


Figure 15: Relation curve of parameter (A) and (B) and axial force (double-tenon joint without auxiliary pretightening device).

Table 4: Empirical formula of bending stiffness for grouted double mortise-tenon joint.

| Joint types | Empirical formulas |
|---|---|
| Without auxiliary pretightening device | $k_\theta = A \cdot e^{(B-M/A)}, \begin{pmatrix} A = 0.106 \cdot N + 38.537 \\ B = 0.9272 \cdot N + 563.19 \end{pmatrix}$ |
| Auxiliary pretightening device in tension side | $k_\theta = A \cdot e^{(B-M/A)}, \begin{pmatrix} A = 0.1271 \cdot N + 64.117 \\ B = 1.1711 \cdot N + 800 \end{pmatrix}$ |

## 5. Conclusion

This paper analyzes the loading test data of 1 : 1 prototype joint under the combined action of axial force and bending moment for various types of grouted double-tenon joints and obtains the basic law of bending stiffness characteristics of grouted double-tenon joint based on the $M$–$\theta$ curve under different axial loads and bending moment. The main conclusions are as follows:

(a) The test study reveals that the double-tenon joints have variable stiffness characteristics. The joint also shows different joint stiffness properties under different load atmosphere. The stiffness changes with the change of axial force and bending moment. For the same type of joint, with the increase of axial force, the bearing capacity and bending stiffness of the joint increase.

(b) Under the action of constant axial force, the stiffness is closely related to the loading moment. The $M$–$\theta$ curve presents a three-stage development of linear stage-nonlinear stage-joint instability stage. The bending stiffness decreases with the increase of bending moment. As the load exceeds the resistance moment, the linear stage ends, cracks appear, and the cracking of joint correspondingly reduces the bearing height characteristics of the bearing section. At this time, the nonlinearity of material results in the attenuation of bending stiffness.

(c) On the whole, the setting of auxiliary pretightening device in tension side is helpful to improve the bending bearing capacity of the joint. However, the auxiliary pretightening device in compression side forms a negative moment in compression side, which reduces the bending stiffness in the early stage of loading. The auxiliary pretightening device in tension side provides additional resistance moment, delays the deterioration process of the joint, and improves the ductility of the joint.

(d) The empirical formulas for calculating the bending stiffness of different types of double-tenon joints with different axial loads and bending moments are obtained, which is helpful for the design and calculation of similar joints in the future.

## Data Availability

The data used to support the findings of this study are available from the corresponding author upon request.

## Conflicts of Interest

The authors declare that they have no conflicts of interest.

## Authors' Contributions

Xiuren Yang supervised the project and developed the concept and methodologies with Meiqun Huang. Fang Lin performed the experimental and theoretical studies.

## Acknowledgments

This research was funded by the National Key S&T Special Projects, under Grant no. 2017YFB1201104.

## References


[1] L. Rozsa, "Precast concrete segment lining of the budapest metro," *Tunnels & Tunnelling International*, vol. 11, no. 10, 1979.

[2] K. Beilasov, Q. H. Qian, and C. Z. Qi, *The Essence of the Construction of Russian Underground Railway*, China Railway Press, Beijing, China, 2012.

[3] J. H. Liu and X. Y. Hou, "The history of shield tunneling," *Shield Tunneling*, pp. 4-5, China Railway Press, Beijing, China, 1991.

[4] H. Backmann and A. Steinle, *Precast Concrete Structures*, Ernst & Sohn, Berlin, Germany, 2011.

[5] X. R. Yang, M. Q. Huang, and F. Lin, "Research strategies on new prefabricated technology for underground metro stations," *Urban Rail Transit*, vol. 5, no. 3, pp. 1–10, 2019.

[6] X. R. Yang, Z. H. Shi, and F. Lin, "Influence of geometrical parameters on performance of grouted mortise and tenon joints for application in prefabricated underground structures," *Advances in Civil Engineering*, vol. 2019, Article ID 3747982, 14 pages, 2019.

[7] X. R. Yang, Z. H. Shi, and F. Lin, "Research on shear capacity and checking method of MT·G-joint for application in prefabricated underground structures," *Advances in Materials Science and Engineering*, vol. 201912 pages, Article ID 4065301, 2019.

[8] S. T. Song, "Experimental study and theoretical analysis in bending and joint shear of high-speed railway precast segmental concrete box bridges," Doctoral Dissertation, Southeast University, Dhaka, Bangladesh, 2015.

[9] J. S. Chen and H. O. Mo, "Three-dimensional fem analysis on flexural rigidity of segment joints in shield tunnel," *Journal of the China Railway Society*, vol. 4, pp. 87–91, 2009.

[10] Z. G. Yan, H. H. Zhu, and S. M. Liao, "A study on performance of steel fiber reinforced concrete segment," *Chinese Journal of Rock Mechanics and Engineering*, vol. 25, no. s1, pp. 2888–2893, 2006.

[11] L. T. Wu, "FEM analysis on mechanical behaviors of segment joints of shield tunnel," Doctoral Dissertation, Southwest Jiaotong University, Chengdu, China, 2005.

[12] R. Gao, K. Zhou, W. Liu, and Q. Ren, "Correlation between the pore structure and water retention of cemented paste backfill using centrifugal and nuclear magnetic resonance methods," *Minerals*, vol. 10, no. 7, p. 610, 2020.

[13] R. Gao, Y. Luo, and H. Deng, "Experimental study on repair of fractured rock mass by microbial induction technology," *Royal Society open science*, vol. 6, no. 11, Article ID 191318, 2019.

[14] X. Luo, P. Cao, Q. Lin, and S. Li, "Mechanical behaviour of fracture-filled rock-like specimens under compression-shear loads: an experimental and numerical study," *Theoretical and Applied Fracture Mechanics*, vol. 113, Article ID 102935, 2021.

[15] J. Hu, G. Wen, Q. Lin, P. Cao, and S. Li, "Mechanical properties and crack evolution of double-layer composite rock-like specimens with two parallel fissures under uniaxial compression," *Theoretical and Applied Fracture Mechanics*, vol. 108, Article ID 102610, 2020.

[16] X. R. Yang and F. Lin, "Prefabrication technology for underground metro station structure," *Tunnelling and Underground Space Technology*, vol. 108, Article ID 103717, 2021.